



## Original Articles

# USP7-mediated ER $\beta$ stabilization mitigates ROS accumulation and promotes osimertinib resistance by suppressing PRDX3 SUMOylation in non-small cell lung carcinoma



Yunchong Meng <sup>a,1</sup>, Wei Lin <sup>a,1</sup>, Na Wang <sup>b,1</sup>, Xiao Wei <sup>c</sup>, Peiyuan Mei <sup>a</sup>, Xiaojun Wang <sup>a</sup>, Chi Zhang <sup>a</sup>, Quanfu Huang <sup>a,\*</sup>, Yongde Liao <sup>a,\*</sup>

<sup>a</sup> Department of Thoracic Surgery, Union Hospital, Tongji Medical College, Huazhong University of Science and Technology, Wuhan, Hubei, 430022, China

<sup>b</sup> Department of Pathology, Union Hospital, Tongji Medical College, Huazhong University of Science and Technology, Wuhan, Hubei, 430022, China

<sup>c</sup> Cancer Biology Research Center (Key Laboratory of the Ministry of Education), Tongji Hospital, Tongji Medical College, Huazhong University of Science and Technology, Wuhan, Hubei, 430030, China

## ARTICLE INFO

**Keywords:**  
NSCLC  
Osimertinib resistance  
ER $\beta$   
ROS accumulation

## ABSTRACT

Osimertinib resistance is regarded as a major obstacle limiting survival benefits for patients undergoing treatment of epidermal growth factor receptor (EGFR)-mutant non-small cell lung cancer (NSCLC). However, the underlying mechanisms of acquired resistance remain unclear. In this study, we report that estrogen receptor  $\beta$  (ER $\beta$ ) is highly expressed in osimertinib-resistant NSCLC and plays a pivotal role in promoting osimertinib resistance. We further identified ubiquitin-specific protease 7 (USP7) as a critical binding partner that deubiquitinates and upregulates ER $\beta$  in NSCLC. ER $\beta$  promotes osimertinib resistance by mitigating reactive oxygen species (ROS) accumulation. We found that ER $\beta$  mechanistically suppresses peroxiredoxin 3 (PRDX3) SUMOylation and thus confers osimertinib resistance onto NSCLC. Furthermore, we provide evidence showing that depletion of ER $\beta$  induces ROS accumulation and reverses osimertinib resistance in NSCLC both in vitro and in vivo. Thus, our results demonstrate that USP7-mediated ER $\beta$  stabilization suppresses PRDX3 SUMOylation to mitigate ROS accumulation and promote osimertinib resistance, suggesting that targeting ER $\beta$  may be an effective therapeutic strategy to overcome osimertinib resistance in NSCLC.

## 1. Introduction

Lung cancer is the second prevalent malignancies and the leading cause of cancer-related death worldwide [1,2]. Non-small cell lung cancer (NSCLC) is the most frequent histological subtype of lung cancer, accounting for approximately 80 % of all patients [1,2]. Despite the continuous refinement of treatment options, the 5-year survival rate still remains about 26.5 % [3]. Development of EGFR-TKIs based on the discovery of EGFR-activating mutations (exon 19 deletion and exon 21 L858R mutation) has dramatically revolutionised the treatment landscape of NSCLC. The frequency of EGFR-activating mutations among Asian NSCLC populations is approximately 50 %, and it is 10–15 % in Europe [4]. As an irreversible third-generation EGFR-TKI, osimertinib has been approved as a first-line therapy in advanced NSCLC patients

harboring EGFR-activating or T790 M resistance mutations [5]. Unfortunately, responses to osimertinib are frequently transient and acquired resistance eventually occurs, which poses a significant challenge due to the paucity of post-osimertinib pharmacological options available to date. Therefore, the elucidation of underlying resistance mechanisms in NSCLC and identification of novel targets to overcome acquired resistance to osimertinib are highly desirable and urgently needed in the clinic.

The modulation of reactive oxidative species (ROS) accumulation in cancer cells has garnered considerable attention [6]. ROS is generally considered important byproducts of oxygen consumption and cellular metabolism in mitochondria [7]. The most common ROS species is hydrogen peroxide ( $H_2O_2$ ) [8]. Following production triggered by exogenous factors, such as chemotherapy, excessive intracellular ROS induce cell death signaling, such as the activation of apoptosis [9]. In

\* Corresponding author.

\*\* Corresponding author.

E-mail addresses: [huangquanfu0527@126.com](mailto:huangquanfu0527@126.com) (Q. Huang), [liaoyongde@hust.edu.cn](mailto:liaoyongde@hust.edu.cn) (Y. Liao).

<sup>1</sup> Yunchong Meng, Wei Lin, and Na Wang contributed equally to the work.

## Abbreviations

EGFR	Epidermal growth factor receptor
EGFR-TKI	Epidermal growth factor receptor tyrosine kinase inhibitors
NSCLC	Non-small cell lung cancer
IHC	Immunohistochemistry
ROS	Reactive oxygen species
Co-IP	Co-immunoprecipitation
ER $\beta$	Estrogen receptor $\beta$
PRDX3	Peroxiredoxin 3
USP7	Ubiquitin-specific protease 7
$\Delta\Psi_m$	Mitochondrial membrane potential
NAC	N-Acetyl-L-cysteine;
PTM	Posttranslational modifications
UBC9	Ubiquitin-Conjugating Enzyme 9
LC-MS/MS	Liquid chromatography tandem-mass spectrometry
IC <sub>50</sub>	Half maximal inhibitory concentration
UPS	ubiquitin–proteasome

response to elevated ROS levels, antioxidant defenses are activated to prevent the build-up of excessive ROS, which contribute to cancer cell survival [10]. Among these defense systems, peroxiredoxins (PRDXs) play crucial roles [11]. PRDX3 protects cells from excess ROS accumulation by eliminating approximately 90 % of cellular H<sub>2</sub>O<sub>2</sub> [12]. Recent studies suggest that posttranslational modifications (PTMs) are very important for modulating the biological functions of PRDX3 [12–14]. Interestingly, SUMOylation, a key PTM characterized by covalent attachment of small ubiquitin-like modifier (SUMO) proteins to target proteins, is a critical event in the dynamic regulation of drug resistance [15–17]. However, the regulatory mechanism underlying PRDX3 SUMOylation and its effects on ROS accumulation and osimertinib resistance are not clearly understood.

Estrogen receptor  $\beta$  (ER $\beta$ ) has been implicated as a pivotal factor in tumor progression [18–20]. In addition, an increasing body of evidence suggests that subcellular localization is key to characterizing the function of the ER $\beta$  protein [21,22]. Cytoplasmic ER $\beta$ , especially mitochondrial ER $\beta$ , is a poor prognostic factor [23,24]. In addition, mitochondria are major sources of ROS [25]. Therefore, we hypothesize that the ER $\beta$  protein may play an important role in ROS accumulation and osimertinib resistance.

In this study, we aimed to investigate how ER $\beta$  modulates ROS accumulation and osimertinib resistance in NSCLC. We found that the expression of ER $\beta$  protein was significantly higher in osimertinib-resistant NSCLC. Through mechanistic studies, we are the first to identify that USP7 is critical for the deubiquitination and upregulation of ER $\beta$  protein in osimertinib-resistant NSCLC. In addition, ER $\beta$  promoted osimertinib resistance by mitigating ROS accumulation. Depletion of ER $\beta$  induced ROS accumulation and reversed osimertinib resistance in NSCLC. Importantly, we discovered that ER $\beta$  mitigated ROS accumulation and conferred osimertinib resistance by suppressing PRDX3 SUMOylation. These findings suggested that ER $\beta$  may be considered a potential therapeutic target for reversing osimertinib resistance in patients with NSCLC.

## 2. Materials and methods

### 2.1. Cell culture

Human NSCLC cell lines (HCC827 and H1975) and HEK293T were originally obtained from the American Type Culture Collection (ATCC, Manassas, VA, USA). To establish osimertinib-resistant HCC827OR and H1975OR cells, HCC827 (EGFR exon 19 deletion) and H1975 (EGFR

L858R and T790 M mutations) cells were exposed to gradually elevated concentrations (10nM–5 $\mu$ M) of osimertinib for six months. All cell lines were cultured in either RPMI-1640 or DMEM (Gibco, NY, USA) supplemented with 10 % FBS (Gibco, NY, USA) and antibiotics (100 units/ml penicillin and 100  $\mu$ g/mL streptomycin) at 37 °C in a humidified atmosphere with 5 % CO<sub>2</sub>.

### 2.2. Antibodies and reagents

The complete information on all the antibodies and reagents used in this study is provided in [Supplementary Tables 1 and 2](#)

### 2.3. Plasmid construction and transfection

All plasmids were constructed by subcloning constructs into a pCDNA3.1 entry vector that were then transferred to a destination vector with or without Flag, HA, and His tags by Gateway Technology (Invitrogen, USA). All mutations were verified by DNA sequencing. Transfection plasmids were performed using X-tremeGENE HP DNA Transfection Reagent (Roche, Switzerland) according to the manufacturer's instructions.

### 2.4. SiRNA transfections

SiRNA transfections were performed using Lipofectamine 3000 transfection reagent (Thermo Fisher Scientific, USA) according to the manufacturer's instructions. SiRNA of PRDX3, USP7, ER $\beta$ , and negative control siRNA (siControl) were provided in [Supplementary Table 3](#).

### 2.5. RNA isolation and real-time quantitative PCR

The total RNA was isolated from cells by a total RNA extraction kit (CAT#DP419, TIANGEN). cDNA was synthesized using a cDNA synthesis kit (CAT#K1622, Thermo Fisher Scientific) on an RT-PCR System (Bio-Rad, USA). Real-time PCR was performed on a CFX Connect quantitative real-time PCR System (Bio-Rad, USA) using SYBR Green Master Mix (Vazyme; cat#R223-01). PCR was carried out in triplicate and standard deviations representing experimental errors were calculated. Pairs of PCR primers used to amplify the target genes are presented in [Supplementary Table 4](#).

### 2.6. Generation of ER $\beta$ knockout cells via the CRISPR/Cas9 system

Lentiviruses of CRISPR sgRNAs targeting human ER $\beta$  were constructed by GeneChem Co., Ltd (Shanghai, China) and used to infect HCC827OR or H1975OR cells. Stable knockout cells were selected with puromycin (2  $\mu$ g/ml) and validated by Western blotting. The sgRNA sequences targeting ER $\beta$  used in our study were as follows:

sgRNA#1, 5'-TGTATATGGAGCCGTGCTCC-3'; sgRNA#2, 5'- CGTT GCGCCAGCC.

CTGTTAC-3', and sgRNA#3, 5'- TAGCGATCTTGCTTCACACC-3'. The sequences Negative control siRNA: sgRNA-NC, 5'-CGCTTCCGGGCC CGITCAA-3'.

### 2.7. RNA sequencing and analysis

Total RNA was isolated using TRIzol reagents (Invitrogen) in accordance with standard manufacturer's protocols. For RNA-sequence analysis, total RNA was sent to the Majorbio (Shanghai, China) for sequencing using the Illumina NovaSeq6000 sequencing platform. According to the  $| \log_2 \text{Ratio} | \geq 1$  and  $p$  value  $< 0.05$  difference standards, edgeR was used to screen for differential genes. GO analysis was conducted using the online platform of Majorbio Cloud Platform.

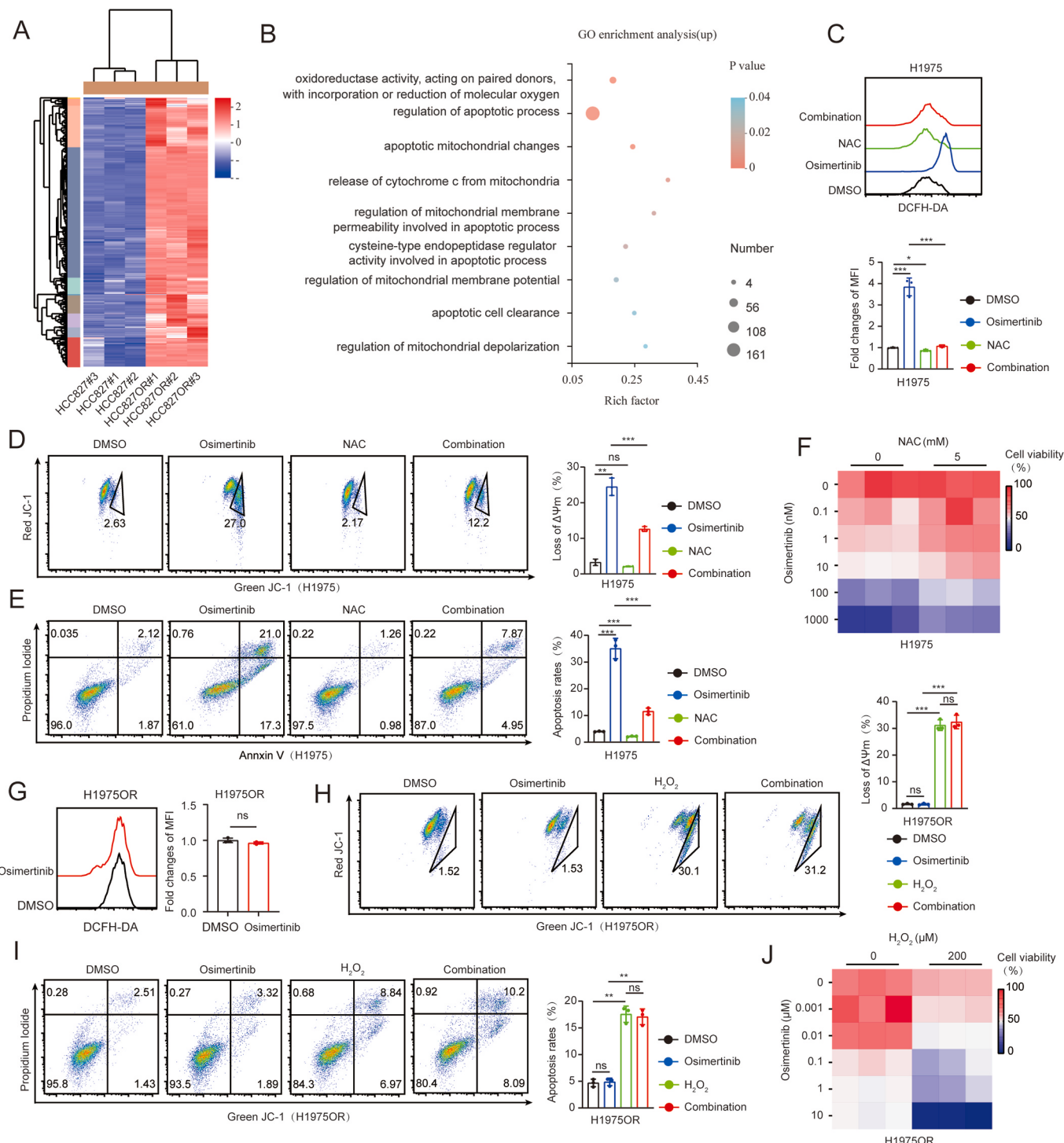
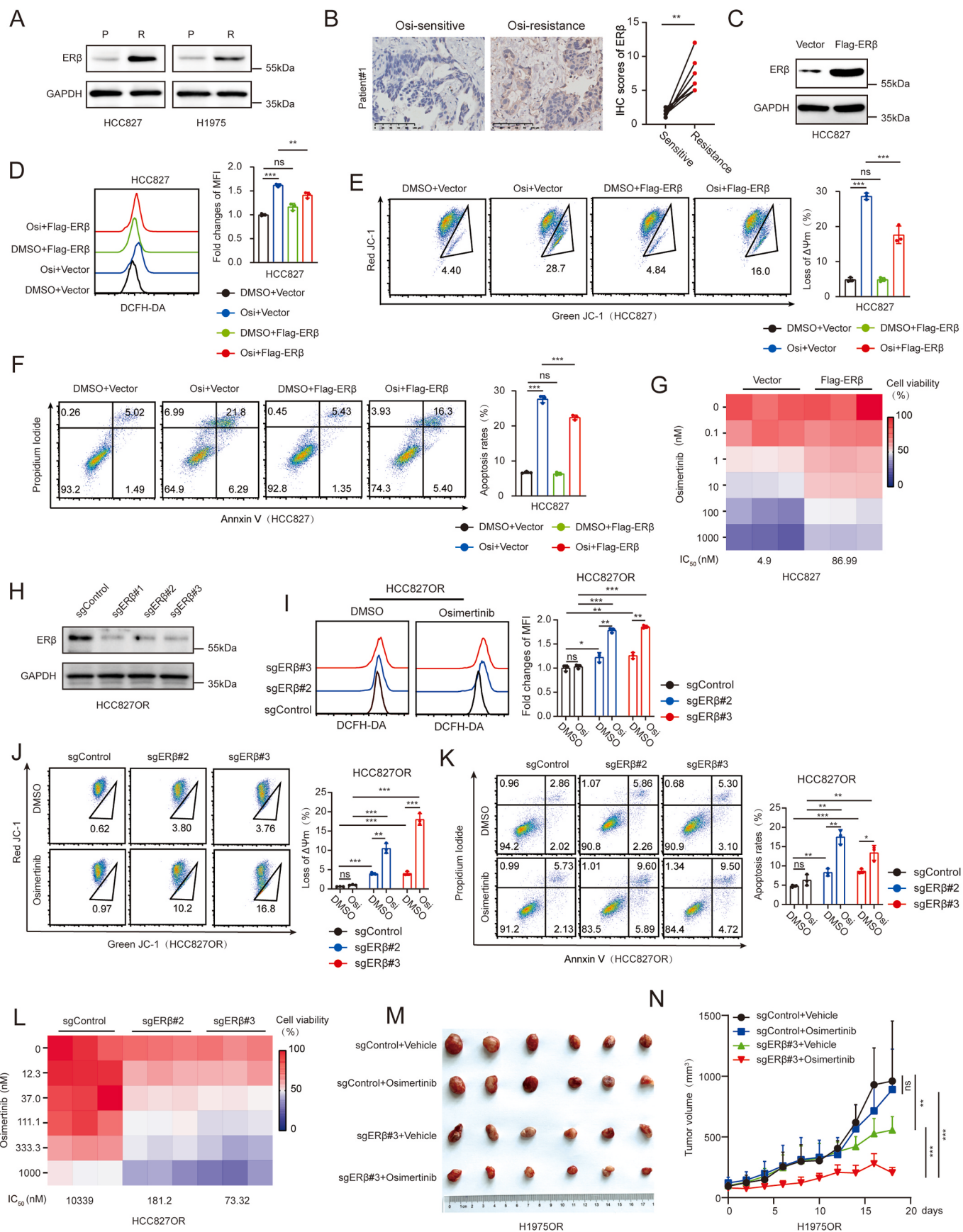


**Fig. 1.** Promoting ROS accumulation overcomes osimertinib resistance in NSCLC.

(A) Heatmap representation of differentially expressed genes in HCC827 and HCC827OR cells. (B) Gene Ontology (GO) analysis showing significant enrichment of upregulated genes in HCC827OR cells. (C-E) H1975 cells were treated with DMSO, osimertinib (100 nM), N-acetyl-cysteine (NAC, 5 mM), or combination for 48 h, respectively. Then, these cells were collected for DCFH-DA (C), JC-1 (D), and Annexin-V/PI (E) flow cytometry assays. (F) H1975 cells were treated with or without a serial dose of osimertinib and NAC (5 mM) for 48 h. Then, these cells were collected for CCK-8 assay. (G) H1975OR cells were treated with DMSO, or osimertinib (1 μM) for 48 h. Then, these cells were collected for DCFH-DA flow cytometry assays. (H, I) H1975OR cells were treated with DMSO, osimertinib (100 nM), H<sub>2</sub>O<sub>2</sub> (200 μM), or combination for 48 h. Then, these cells were collected for JC-1 (H) and Annexin-V/PI (I) flow cytometry assays. (J) H1975OR cells were treated with or without a serial dose of osimertinib and H<sub>2</sub>O<sub>2</sub> (200 μM) for 72 h. Then, these cells were collected for CCK-8 assay. Error bars represent the mean ( $n = 3$ )  $\pm$  S.D. ns > 0.05, \*p < 0.05, \*\*p < 0.01, and \*\*\*p < 0.001.



(caption on next page)

**Fig. 2.** ER $\beta$  contributes to osimertinib resistance by mitigating ROS accumulation.

(A) The expression of ER $\beta$  protein in osimertinib-resistant cells and parental cells was measured via Western blot. (B) Immunohistochemistry detection and quantification of ER $\beta$  in matched tumor specimens before and after resistance to osimertinib (Osi) treatment in NSCLC cells. Scale bar = 20  $\mu$ m. (C) HCC827 cells were transfected with vector or Flag-ER $\beta$  plasmids, and the expression of ER $\beta$  protein was measured via Western blot. (D–F) HCC827 cells were transfected with vector or Flag-ER $\beta$  plasmid for 72 h and treated with or without osimertinib (Osi, 100 nM) for another 48 h. Then, these cells were collected for DCFH-DA (D), JC-1 (E), and Annexin-V/PI (F) flow cytometry assays. (G) HCC827 cells were transfected with vector or Flag-ER $\beta$  plasmid for 72 h and treated with a serial dose of osimertinib. Then, these cells were collected for CCK-8 assay and subjected to measure the IC<sub>50</sub> values of osimertinib. (H) ER $\beta$  was knocked out in HCC827OR cells using the indicated sgRNAs. (I–K) HCC827OR cells were transfected with sgControl or sgER $\beta$  and treated with DMSO or osimertinib (1  $\mu$ M) for 48 h. Then, these cells were collected for DCFH-DA (I), JC-1 (J), and Annexin-V/PI (K) flow cytometry assays. (L) HCC827OR cells were transfected with sgControl or sgER $\beta$  and treated with a serial dose of osimertinib. Then, these cells were collected for CCK-8 assay and subjected to measure the IC<sub>50</sub> values of osimertinib. (M, N) H1975OR cells were transfected with sgControl or sgER $\beta$  and implanted into the right hind limbs of mice ( $n = 6$  per group). After palpable tumors formed, a vehicle (10 % dimethyl sulfoxide (DMSO) and 90 % corn oil, oral gavage) or osimertinib (5 mg/kg, oral gavage) was administered once per 2 days. Tumor volumes were measured every 2 days. Tumors were harvested and photographed on day 18. Error bars represent the mean ( $n = 3$ )  $\pm$  S.D. ns p > 0.05, \*p < 0.05, \*\*p < 0.01, and \*\*\*p < 0.001.

## 2.8. Apoptosis analysis using flow cytometry

This assay was performed as described previously [26]. Different cell groups were harvested and stained with Annexin-V/propidium iodide (PI) apoptosis kit (BD Biosciences, NJ, USA). Samples were analyzed by FACS Calibur flow cytometer (BD Biosciences, USA).

## 2.9. Measurement of mitochondrial transmembrane potential

According to the manufacturer's instructions of Mitochondrial membrane potential assay kit with JC-1 (Beyotime, China), cells were stained with JC-1 (1  $\times$ ). Samples were analyzed by FACS Calibur flow cytometer (BD Biosciences, USA).

## 2.10. Measurement of ROS

According to the manufacturer's instructions of Reactive Oxygen Species Assay Kit (Beyotime, China), cells were stained with DCFH-DA (1  $\times$ ). Samples were analyzed by FACS Calibur flow cytometer (BD Biosciences, USA).

## 2.11. Immunofluorescence and confocal microscopy

Cells were seeded into the uncoated 35-mm dishes. After 24 h, the medium was replaced with fresh media containing 100 nM MitoTracker Red CMXROS (Beyotime, China) at 37 °C for 15 min. Cells were washed in cold PBS, fixed with 4 % polyoxymethylene, permeabilized with 0.25 % Triton™ X-100, blocked with 5 % bovine serum albumin (BSA), and incubated with primary antibodies against ER $\beta$  overnight at 4 °C. Highly cross-adsorbed secondary antibody was used to label the cells at 37 °C for 1 h, and then the cells were counterstained with DAPI. Images were acquired using a Confocal Microscope (Olympus, Tokyo, Japan).

## 2.12. Immunohistochemistry (IHC)

The tumors were harvested and fixed in 4 % Polyformaldehyde, embedded in paraffin and sectioned into 4- $\mu$ m thick. The tissue sections were analyzed by IHC staining as previously described [27].

## 2.13. Western blotting and immunoprecipitation

Western blotting and immunoprecipitation cell lysates were prepared using NP40 buffer and resolved by SDS-PAGE for Western blotting. The cell extracts were initially incubated overnight with A/G Magnetic Beads (MCE, USA) at 4 °C for exogenous immunoprecipitation. For endogenous binding, cell lysates were incubated with Flag (MCE, USA), HA (MCE, USA), and His magnetic beads (Biolinkedin, China) overnight. Lysates were then washed with NP40 buffer five times prior to Western blotting analysis.

## 2.14. In vivo ubiquitination assay

Transfection of indicated plasmids into cells was carried out prior to the addition of 20  $\mu$ M proteasome inhibitor MG132 for 8 h prior to harvesting. Cells were lysed using NP40 buffer. Flag Magnetic Beads (MCE, USA) was then added and put on a rotating incubator overnight at 4 °C. The beads were then washed five times with NP40 buffer, boiled with SDS loading buffer and ubiquitinated ER $\beta$  was detected by Western blot with anti-HA antibody.

## 2.15. GST-pull down assay

Flag-ER $\beta$  plasmid was transfected into HEK293T cells for 24 h, and then the cell lysates were incubated with purified GST-only (Abclonal, China) or GST-USP7 (Sinobiological, China) fusion proteins plus GST Magnetic Beads (biolinkedin, China) overnight. Lysates were then washed with NP40 buffer five times prior to Western blotting analysis.

## 2.16. Liquid chromatography tandem-mass spectrometry (LC-MS/MS) analysis

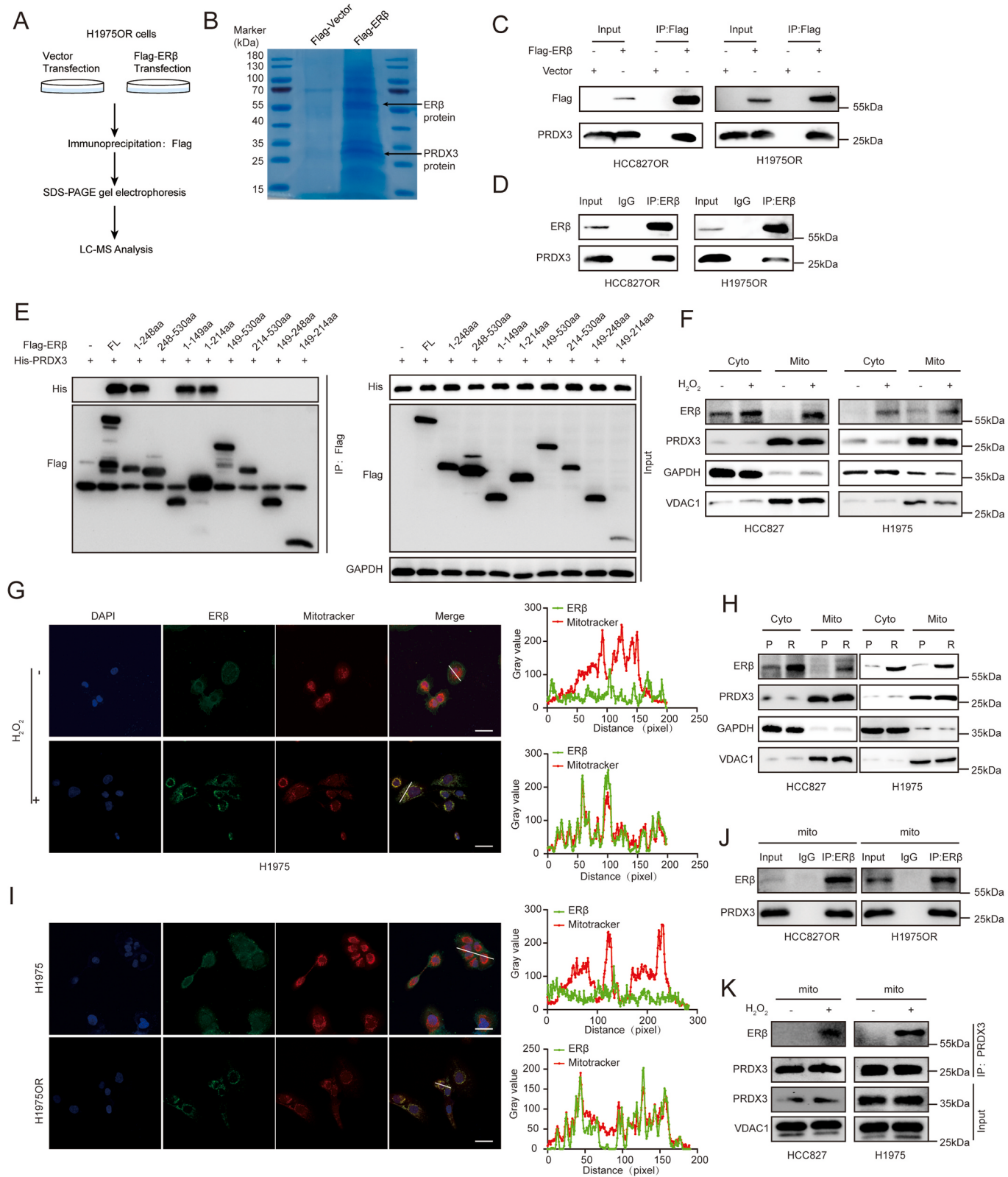
H1975OR cells transfected with Flag-ER $\beta$ -expressing plasmid were used to identify ER $\beta$ -binding proteins. Flag-ER $\beta$  was immunoprecipitated using the Flag Magnetic Beads (MCE, USA) overnight at 4 °C. The immunocomplexes were subjected to Western blotting. Protein bands were excised and further analyzed by LC-MS/MS (performed by National Protein Science Facility, School of Life Science, Tsinghua University).

## 2.17. Mouse xenograft model

All animal experiments were performed with the approval of the Medical Ethics Committee of Tongji Medical College, Huazhong University of Science and Technology. Female BALB/c-nu mice (5 weeks old) were randomly assigned to four groups (six mice per group). A total of  $2 \times 10^6$  H1975OR stable cells (sgControl, sgER $\beta$ #3) were subcutaneously injected into these mice. After palpable tumors formed, a vehicle (10 % dimethyl sulfoxide (DMSO) and 90 % corn oil, oral gavage) or osimertinib (5 mg/kg, oral gavage) was administered once per 2 days. For 2-D08 treatment,  $2 \times 10^6$  H1975 cells were subcutaneously injected into female BALB/c-nu mice (5 weeks old). After palpable tumors formed, the mice were randomly assigned to three groups, and a vehicle (10 % DMSO and 90 % corn oil, oral gavage), osimertinib (5 mg/kg, oral gavage), or a combination of osimertinib and 2-D08 (10 mg/kg, intraperitoneal injection) was administered once per 2 days. Tumor growth and body weight were monitored every 2 days. The tumor size was measured with a slide caliper, and tumor volumes were calculated using the following formula: volume = length  $\times$  width<sup>2</sup>  $\times$  0.5.

## 2.18. Statistical analysis

An unpaired two-tailed Student's *t*-test was performed when two



(caption on next page)

groups were compared. Comparisons between multiple groups were performed with a one-way ANOVA and Bonferroni post hoc test. All results were recorded as the mean  $\pm$  SD (standard deviation). The data were analyzed using GraphPad Prism 9 (GraphPad Software, Inc.) with

the P values. Biological triplicates or duplicates were established and at least three independent experiments with similar results were performed.  $p < 0.05$  was considered statistically significant. In the figures, \*, \*\*, and \*\*\* refer to  $p < 0.05$ ,  $p < 0.01$ , and  $p < 0.001$ , respectively.

**Fig. 3.** ROS induces the translocation of ER $\beta$  to mitochondria and promotes the ER $\beta$ -PRDX3 protein interaction. (A) Extracts of H1975OR cells transfected with vector or Flag-ER $\beta$  were immunoprecipitated with an anti-Flag antibody. Eluted proteins were identified by LC-MS analysis. (B) Eluted proteins were separated by SDS-PAGE and visualized by Coomassie blue staining. (C) Extracts of HCC827OR and H1975OR cells transfected with vector or Flag-ER $\beta$  plasmids were immunoprecipitated with anti-Flag magnetic beads. (D) Extracts of HCC827OR and H1975OR cells were immunoprecipitated with IgG and ER $\beta$  antibodies. (E) Extracts of HEK293T cells transfected with functional truncations of Flag-ER $\beta$  plasmids (1-248aa, 248-530aa, 1-149aa, 1-214aa, 149-530aa, 214-530aa, 149-248aa, or 149-214aa) or His-PRDX3 plasmids were immunoprecipitated with anti-Flag magnetic beads. (F) The expression of the indicated proteins in mitochondria and mitochondrial-free cytosolic fractions of HCC827 and H1975 cells treated with H<sub>2</sub>O<sub>2</sub> (200  $\mu$ M) for 120 min was measured. (G) Confocal microscopy was used to observe the colocalization of endogenous ER $\beta$  and mitochondria in H1975 cells treated with H<sub>2</sub>O<sub>2</sub> (200  $\mu$ M) for 120 min, scale bar = 20  $\mu$ m. Plot profile qualitative analysis was used to describe the co-localization status. (H) The expression of the indicated proteins in mitochondria and mitochondrial-free cytosolic fractions of osimertinib-resistant and parental cells was detected. (I) Confocal microscopy was used to observe the colocalization of endogenous ER $\beta$  and mitochondria in H1975 and H1975OR cells, scale bar = 20  $\mu$ m. Plot profile qualitative analysis was used to describe the co-localization status. (J) Mitochondrial extracts from HCC827OR and H1975OR cells exposed to H<sub>2</sub>O<sub>2</sub> (200  $\mu$ M) for 120 min were immunoprecipitated with PRDX3 antibody.

### 3. Results

#### 3.1. Promoting ROS accumulation overcomes osimertinib resistance in NSCLC

ROS accumulation is recognized as a key player in cell survival [28]. However, the roles of ROS accumulation in osimertinib resistance remain puzzling. To elucidate the mechanism underlying this resistance, we established osimertinib-resistant NSCLC cells, which exhibited greater half maximal inhibitory concentration (IC<sub>50</sub>) values compared to the parental cells (Figs. S1A and B). RNA-sequence and Gene Ontology (GO) analysis revealed that osimertinib-resistant NSCLC cells were involved mainly in the regulation of oxidative stress, mitochondrial dysfunction, and cell apoptosis (Fig. 1A and B). Enhanced ROS-mediated oxidative damage causes cellular oxidative stress [29].

Changes in the mitochondrial membrane potential ( $\Delta\Psi_m$ ) are used to measure of mitochondrial function, which is often compromised by oxidative stress [30,31]. Hence, DCFH-DA and JC-1 assays showed that osimertinib treatment elevated ROS levels and caused loss of  $\Delta\Psi_m$  in HCC827 and H1975 cells (Fig. 1C, D and S1C, D). There is a close connection between  $\Delta\Psi_m$  and cell apoptosis [32]. Thus, we next performed Annexin-V/PI assays, which showed that osimertinib significantly induced cell apoptosis (Fig. 1E and S1E). Although osimertinib induces ROS accumulation in osimertinib-sensitive NSCLC, it is unclear whether enhanced ROS causes osimertinib-mediated  $\Delta\Psi_m$  and cell apoptosis. Thus, we applied the ROS production inhibitor, N-acetylcysteine (NAC). Notably, NAC significantly inhibited osimertinib-induced ROS accumulation and loss of  $\Delta\Psi_m$  (Fig. 1C,D and S1C,D). Annexin-V/PI assays exhibited that NAC plus osimertinib treatment significantly reduced cell apoptosis compared to osimertinib treatment alone (Fig. 1E and S1E). Moreover, CCK-8 assays showed that NAC weakened the inhibitory effect of osimertinib on NSCLC cell proliferation (Fig. 1F and S1F). Thus, these results indicate that osimertinib induces cell death by promoting ROS accumulation in osimertinib-sensitive NSCLC cells.

ROS levels,  $\Delta\Psi_m$ , and cell apoptosis rate were not significantly changed in HCC827OR and H1975OR cells after osimertinib treatment (Fig. 1G-I and S1G-I). However, we found that H<sub>2</sub>O<sub>2</sub>, the major component of ROS, could induce the loss of  $\Delta\Psi_m$  and activated cell apoptosis in HCC827OR and H1975OR cells (Fig. 1H, I and S1H, I). Meanwhile, H<sub>2</sub>O<sub>2</sub> could reverse the resistance to osimertinib (Fig. 1J and S1J). Therefore, these results suggest that promoting ROS accumulation is a viable strategy to overcome osimertinib resistance in NSCLC.

#### 3.2. ER $\beta$ contributes to osimertinib resistance by mitigating ROS accumulation

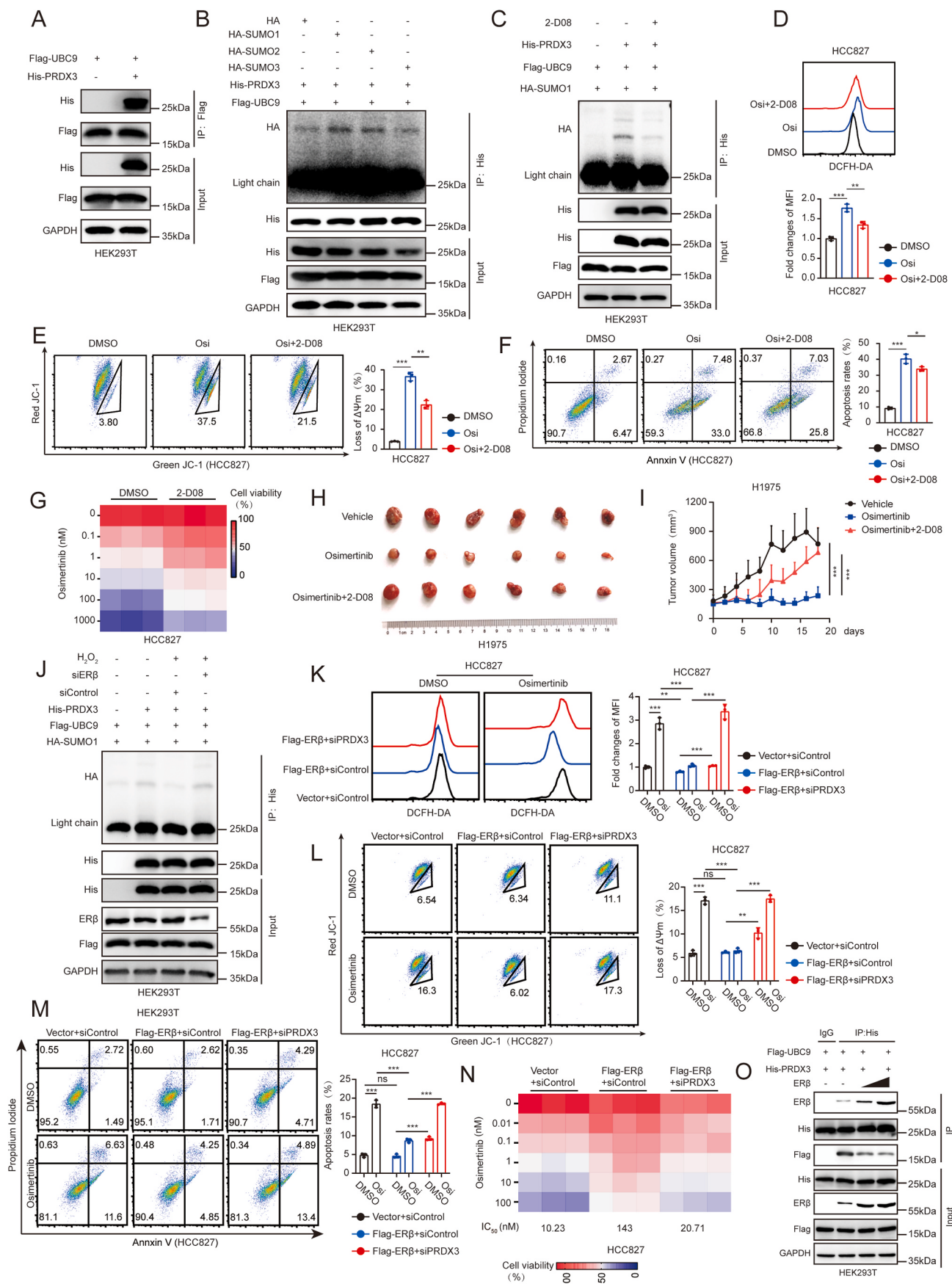
Previous studies clearly showed that ER $\beta$  is an oncogene in NSCLC [18–20,33]. However, the role of ER $\beta$  in osimertinib-resistant NSCLC cells had not been determined to date. Therefore, we first examined the change in ER $\beta$  protein expression in parental and osimertinib-resistant

NSCLC cells. As shown in Fig. 2A, ER $\beta$  protein was overexpressed in osimertinib-resistant cells compared with parental cells. To extend these results to clinical samples, we analyzed matched tumor specimens from seven NSCLC patients before and after they showed resistance to osimertinib. Immunohistochemistry (IHC) results showed that ER $\beta$  protein expression was significantly increased in the osimertinib-resistant specimens (Fig. 2B). More importantly, cytoplasmic ER $\beta$  accumulation was also identified (Fig. 2B). Interestingly, previous studies had identified that cytoplasmic ER $\beta$  is a poor prognostic factor of tumor progression [20,21]. Collectively, these results suggest that the ER $\beta$  protein might promote osimertinib resistance.

To identify whether ER $\beta$  promotes osimertinib resistance, we overexpressed ER $\beta$  protein in HCC827 and H1975 cells (Fig. 2C and S2A). DCFH-DA, JC-1, and Annexin-V/PI assays showed that the ability of osimertinib on increasing ROS levels, causing loss of  $\Delta\Psi_m$ , and inducing cell apoptosis was weakened after ER $\beta$  overexpression (Fig. 2D–F and S2B–D). In addition, ER $\beta$  overexpression in HCC827 and H1975 cells increased the IC<sub>50</sub> for osimertinib (Fig. 2G and S2E). To further evaluated whether ER $\beta$  depletion is effective in overcoming osimertinib resistance, we depleted endogenous ER $\beta$  protein in HCC827OR and H1975OR cells (Fig. 2H and S2F). The results showed that combined ER $\beta$  depletion and osimertinib treatment increased ROS levels to a greater extent than osimertinib treatment alone (Fig. 2I and S2G). As a response to ROS accumulation, osimertinib-caused loss of  $\Delta\Psi_m$  and cell apoptosis was also significantly increased following ER $\beta$  knockout (Fig. 2J,K and S2H,I). Moreover, CCK8 assays exhibited that ER $\beta$  depletion in HCC827OR and H1975OR cells decreased the IC<sub>50</sub> for osimertinib (Fig. 2L and S2J). Next, we examined the effect of ER $\beta$  knockout in xenografts exposed to osimertinib. As shown in Fig. 2M and N, sgER $\beta$  group exposed to osimertinib showed significantly reduced the tumor growth compared to those of the control group exposed only to osimertinib. All together, these data imply that ER $\beta$  promotes osimertinib resistance by mitigating ROS accumulation in NSCLC.

#### 3.3. ROS induces the translocation of ER $\beta$ to mitochondria and promotes the ER $\beta$ -PRDX3 protein interaction

To explore the potential molecular mechanisms by which ER $\beta$  promotes osimertinib resistance, liquid chromatography–tandem mass spectroscopy (LC-MS/MS) assays were performed to identify ER $\beta$ -interacting proteins (Fig. 3A and Dataset.1). Excitingly, PRDX3 was one of the potential ER $\beta$  binding proteins identified (Fig. 3B). As one of the most crucial ROS scavengers, PRDX3 protects cells from ROS accumulation by eliminating cellular H<sub>2</sub>O<sub>2</sub> [34]. Therefore, we presumed that ER $\beta$  regulates ROS accumulation and promotes osimertinib resistance through its interactions with PRDX3. To confirm this interaction, we performed coimmunoprecipitation (co-IP) assays and found that endogenous PRDX3 coprecipitated from cells ectopically expressing ER $\beta$  and that endogenous ER $\beta$  coprecipitated from cells ectopically expressing PRDX3 (Fig. 3C and S3A). Additionally, an endogenous interaction between ER $\beta$  and PRDX3 was observed in NSCLC cells (Fig. 3D and S3B). To map the regions of ER $\beta$  that interacts with PRDX3,



(caption on next page)

**Fig. 4.** ER $\beta$  regulates ROS accumulation and promotes osimertinib resistance through its inhibition of PRDX3 SUMOylation. (A) Extracts of HEK293T cells transfected with Flag-UBC9 and His-PRDX3 were immunoprecipitated with anti-Flag magnetic beads. (B) Extracts of HEK293T cells transfected with indicated plasmids were immunoprecipitated with anti-His magnetic beads. (C) Extracts of HEK293T cells transfected with indicated plasmids and treated with or without 2-D08 (10  $\mu$ M) for 72 h were immunoprecipitated with anti-His magnetic beads. (D–F) HCC827 cells were treated with or without osimertinib (Osi, 100 nM) and 2-D08 (10  $\mu$ M) for 48 h. Then, these cells were collected for DCFH-DA (D), JC-1 (E), and Annexin-V/PI (F) flow cytometry assays. (G) HCC827 cells were treated with or without a serial dose of osimertinib and 2-D08 (10  $\mu$ M) for 72 h. Then, these cells were collected for CCK-8 assays. (H, I) H1975 cells were implanted into the right hind limbs of mice ( $n = 6$  per group). After palpable tumors formed, vehicle (10 % DMSO and 90 % corn oil, oral gavage), osimertinib (5 mg/kg, oral gavage), or combinations of osimertinib and 2-D08 (10 mg/kg, intraperitoneally injected) was administered once per 2 days. Tumor volumes were measured every 2 days. Tumors were harvested and photographed on day 18. (J) HEK293T cells were transfected with plasmids or siRNAs (siControl, siER $\beta$ ) for 72 h and treated with  $H_2O_2$  (200  $\mu$ M) for another 120 min. Then, these cells were harvested and immunoprecipitated with anti-His magnetic beads. (K–M) HCC827 cells were transfected with the indicated plasmids (vector, Flag-ER $\beta$ ) or siRNAs (siControl, siPRDX3) for 72 h and treated with or without osimertinib (100 nM) for another 48 h. Then, these cells were collected for DCFH-DA (K), JC-1 (L), and Annexin-V/PI (M) flow cytometry assays. (N) HCC827 cells were transfected with the indicated plasmids (vector, Flag-ER $\beta$ ) or siRNAs (siControl, siPRDX3) for 72 h and treated with a serial dose of osimertinib. Then, these cells were collected for CCK-8 assay and subjected to measure the IC<sub>50</sub> values of osimertinib. (O) HEK293T cells were transiently co-transfected with Flag-UBC9 and His-PRDX3 plasmids together with increasing amounts of ER $\beta$  plasmids. Cell lysate was subjected to immunoprecipitation with anti-His magnetic beads. Error bars represent the mean ( $n = 3$ )  $\pm$  S.D. ns  $p > 0.05$ , \* $p < 0.05$ , \*\* $p < 0.01$ , and \*\*\* $p < 0.001$ .

we generated eight functional truncations of ER $\beta$  protein (1-248aa, 248-530aa, 1-149aa, 1-214aa, 149-530aa, 214-530aa, 149-248aa and 149-214aa) and found that the A/B domain (1-149aa) in ER $\beta$  binds to PRDX3 (Fig. 3E and S3C). Collectively, these results indicate that ER $\beta$  physically and specifically interacts with PRDX3.

Previous studies verified that PRDX3 localized to mitochondria [35]. Thus, through ROS-induced stimulation, ER $\beta$  may be translocated to mitochondria, where it interacts with PRDX3. To test this hypothesis, we firstly prepared NSCLC cell mitochondrial and mitochondrion-free cytosolic fractions and then detected ER $\beta$  and PRDX3 in each fraction. As shown in Fig. 3F, ROS caused a marked increase in the level of ER $\beta$  in the mitochondrial fraction. Colocalization of endogenous ER $\beta$  and mitochondria was found in H1975 cells after ROS-induced stimulation (Fig. 3G). The level of ER $\beta$  in the mitochondrial fraction of HCC827OR cells was significantly higher than that in the parental cells (Fig. 3H). Although ER- $\beta$  is slightly present in the mitochondria of H1975 cells, the increase of ER- $\beta$  in the mitochondria was significant in H1975OR cells compared to parental cells (Fig. 3H). Consistently, we found colocalization of endogenous ER $\beta$  and mitochondria in H1975OR cells but a lesser degree of colocalization in H1975 cells (Fig. 3I). Consistent with previous studies [36,37], our results confirmed that PRDX3 localized to mitochondria, but few were found in the mitochondrion-free cytosolic fractions (Fig. 3F, H). Our data also showed that the ER $\beta$  protein interacted with PRDX3 in the mitochondrial fraction of osimertinib-resistant cells (Fig. 3J and S3D). Moreover, ROS enhanced the interaction of ER $\beta$  with PRDX3 in the mitochondrial fraction of osimertinib-sensitive cells (Fig. 3K). In summary, these results suggest that ROS stimulate the ER $\beta$  translocation to mitochondria and promote the interaction of ER $\beta$  with PRDX3 in mitochondria.

#### 3.4. ER $\beta$ regulates ROS accumulation and promotes osimertinib resistance through its inhibition of PRDX3 SUMOylation

To explore whether ER $\beta$  promotes osimertinib resistance by regulating PRDX3 expression, we assessed the change in PRDX3 protein level after ER $\beta$  overexpression. Unfortunately, the PRDX3 protein level was not regulated by ER $\beta$  (Fig. S4A). Numerous studies have reported that PRDX3 PTMs play important roles in regulating antioxidative stress [12–14]. SUMOylation, a PTM involving the covalent attachment of SUMO peptides, is involved in the stress response [38]. Therefore, we evaluated the possibility that PRDX3 is SUMOylated. To test this hypothesis, we first performed co-IP with PRDX3 and UBC9, the sole SUMOylation-conjugating enzyme in mammalian cells. The results found an interaction between PRDX3 and UBC9 (Fig. 4A and S4B). Three SUMO proteins, SUMO1, SUMO2 and SUMO3 can be covalently conjugated to the targeted proteins [39]. The co-IP assays showed that PRDX3 was mostly conjugated to SUMO1 and SUMO2 (Fig. 4B). Among these two enzymes, SUMO1 binding to PRDX3 was stronger, indicating that SUMO1 was more important in PRDX3 SUMOylation (Fig. 4B). To

determine the role of PRDX3 SUMOylation in mediating ROS accumulation and osimertinib resistance, the selective SUMOylation inhibitor 2-D08 was used in experiments. As shown in Fig. 4C, PRDX3 SUMOylation was significantly inhibited after 2-D08 treatment. Although ROS levels,  $\Delta\Psi_m$ , and cell apoptosis rate were not significantly changed in NSCLC cells after 2-D08 treatment (Figs. S4C–E), 2-D08 weakened the ability of osimertinib to elevate ROS levels, indicating that PRDX3 SUMOylation suppressed the effect of PRDX3 on ROS elimination (Fig. 4D and S5A). JC-1 and Annexin-V/PI assays showed that 2-D08 partially inhibited the effect of osimertinib on causing the loss of  $\Delta\Psi_m$  and cell apoptosis (Fig. 4E,F and S5B,C). We also performed CCK8 assays to show that 2-D08 treatment significantly reduced osimertinib sensitivity in HCC827 and H1975 cells (Fig. 4G and S5D). Consistent with the in vitro data, the ability of osimertinib to inhibit tumor growth was significantly diminished when osimertinib treatment was combined with 2-D08 (Fig. 4H and I).

Next, we aimed to investigate whether ER $\beta$  mediated PRDX3 SUMOylation. Co-IP assays showed that ER $\beta$  overexpression reduced the PRDX3 SUMOylation (Fig. S5E). Moreover, ER $\beta$  knockdown rescued the ROS-induced decrease in the PRDX3 SUMOylation (Fig. 4J). DCFH-DA assays showed that PRDX3 silencing strengthened the osimertinib-induced ROS accumulation in ER $\beta$ -overexpressed NSCLC cells (Fig. 4K and S5F,G). In addition, the osimertinib-induced loss of  $\Delta\Psi_m$  and increase in the cell apoptosis rate in ER $\beta$ -overexpressed NSCLC cells were also promoted via PRDX3 silencing (Fig. 4L,M and S5Happsec1,I). CCK8 assays also showed that PRDX3 silencing in NSCLC cells with ER $\beta$  overexpression restored the suppressive effects of osimertinib on cell proliferation (Fig. 4N and S5J). Given that UBC9 is the sole SUMOylation-conjugating enzyme and is required for the transfer of SUMO molecules to targeted substrates in mammalian cells [40], the reduction in SUMOylation may have been a result of the impaired affinity of UBC9 for PRDX3 binding due to ER $\beta$  overexpression. As we predicted, the co-IP assays confirmed that an increase in ER $\beta$  competitively inhibited the PRDX3 and UBC9 interaction. (Fig. 4O). Taken together, these results suggest that ER $\beta$  mitigates ROS accumulation and promotes osimertinib resistance through its suppression of PRDX3 SUMOylation.

#### 3.5. ER $\beta$ directly interacts with the deubiquitinase USP7

To identify the mechanism underlying ER $\beta$  upregulation in osimertinib-resistant NSCLC, we performed an LC-MS/MS analysis to identify potential ER $\beta$ -binding molecules (Dataset.1). Among various candidates, the deubiquitinases USP7 and USP10 were shown to potentially bind with ER $\beta$ . Co-IP assays showed that the interaction of ER $\beta$  with USP7 was stronger than that with USP10, indicating that the ER $\beta$ /USP7 interaction was more important (Fig. 5A and B). The endogenous interaction between USP7 and ER $\beta$  was observed in NSCLC cells (Fig. 5C). GST pull-down assays verified that USP7 directly formed a complex with ER $\beta$  (Fig. 5D).

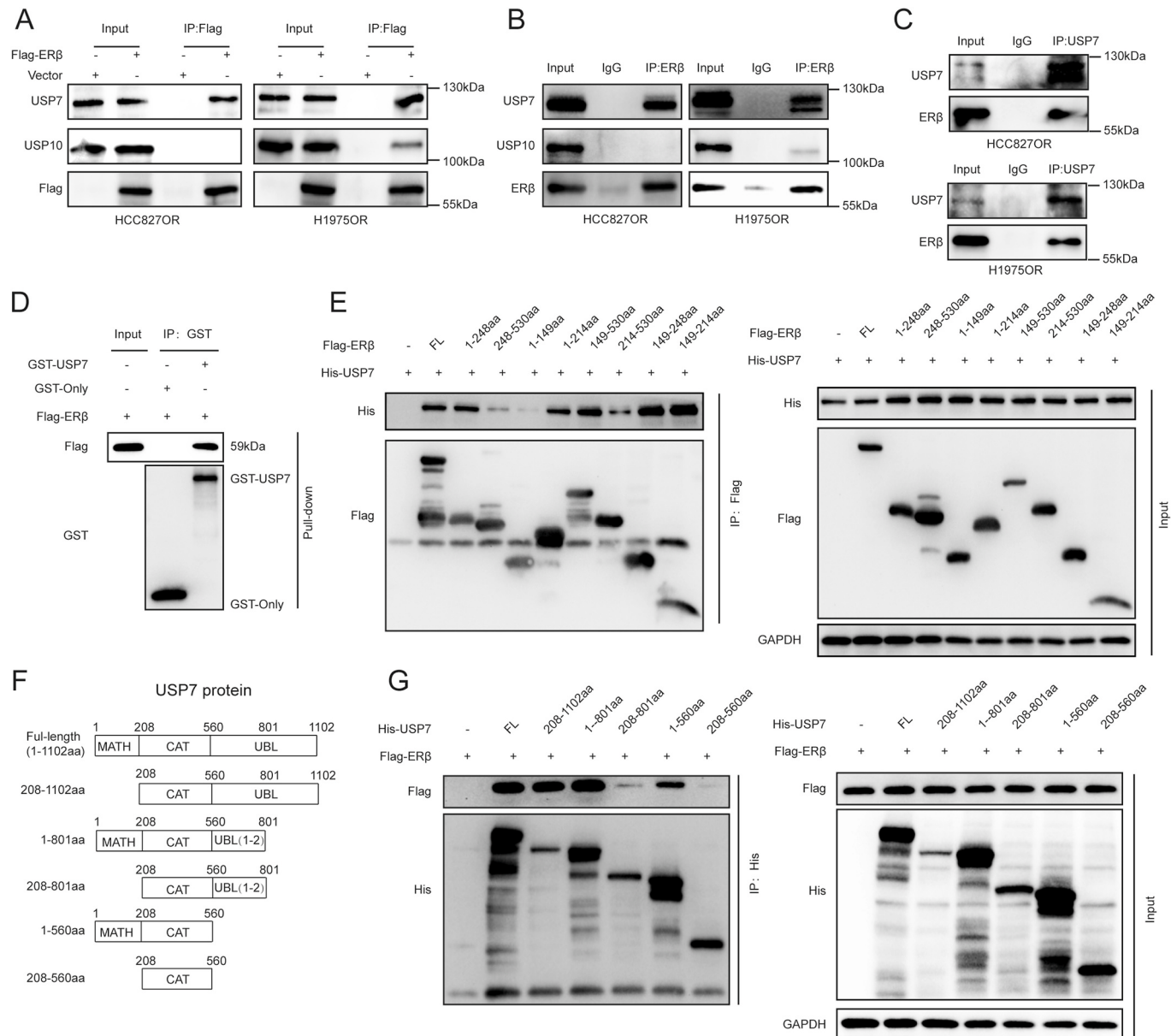
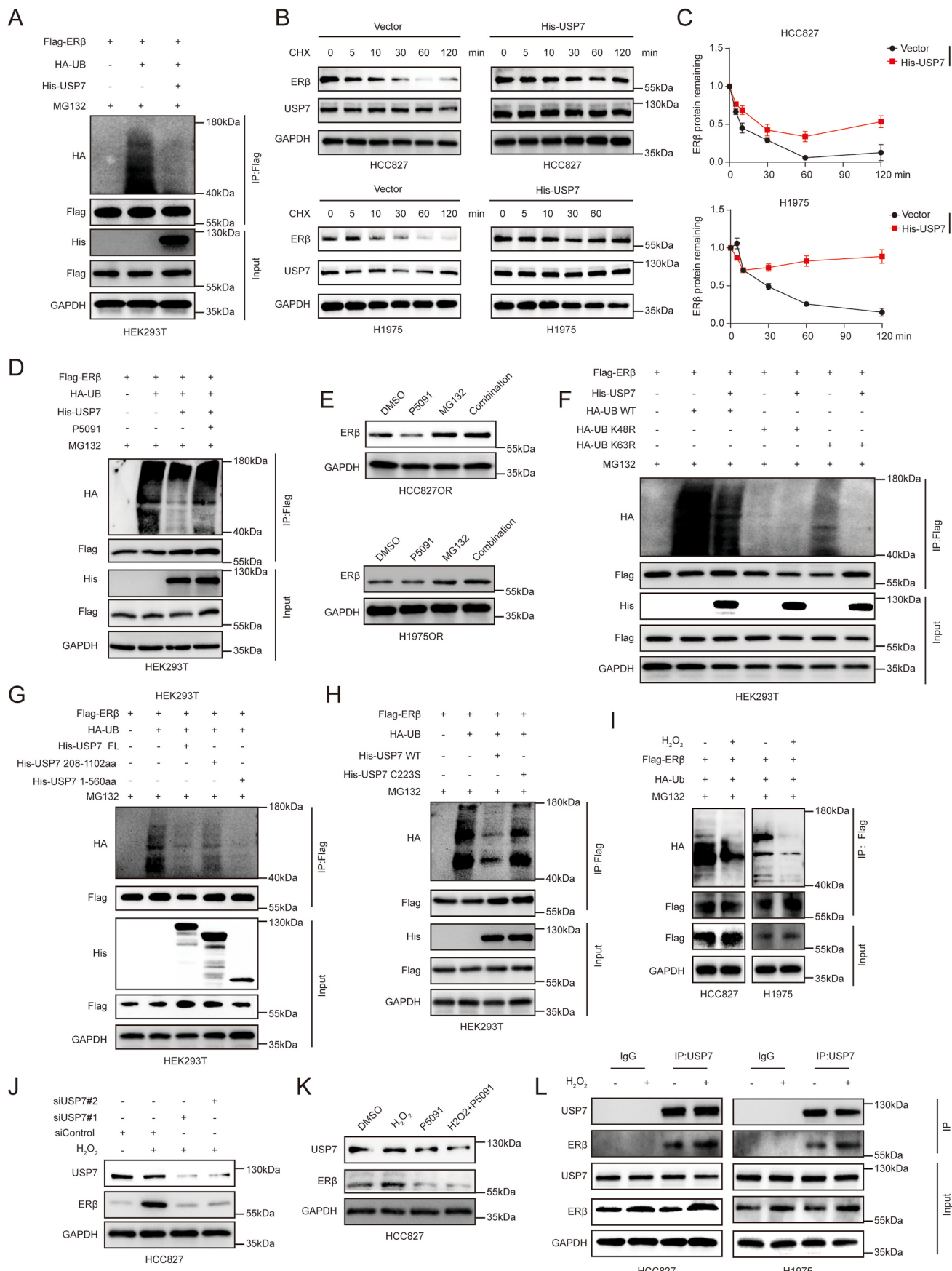


**Fig. 5.** ER $\beta$  directly interacts with the deubiquitinase USP7. (A) Extracts of HCC827OR and H1975OR cells transfected with vector or Flag-ER $\beta$  plasmids were immunoprecipitated with anti-Flag magnetic beads. (B) Extracts of HCC827OR and H1975OR cells were immunoprecipitated with IgG and ER $\beta$  antibodies. (C) Extracts of HCC827OR and H1975OR cells were immunoprecipitated with IgG and USP7 antibodies. (D) Lysate of HEK293T cells transfected with Flag-ER $\beta$  plasmids was subjected to immunoprecipitation with recombinant GST-only or GST-USP7 proteins coupled to GST magnetic beads. (E) Extracts of HEK293T cells transfected with functional truncations of Flag-ER $\beta$  plasmids (1-248aa, 248-530aa, 1-149aa, 1-214aa, 149-530aa, 214-530aa, 149-248aa, or 149-214aa) or His-USP7 plasmids were immunoprecipitated with anti-Flag magnetic beads. (F) The full-length USP7 was divided into five functional truncations (208-1102aa, 1-801aa, 208-801aa, 1-560aa, 208-560aa) and five fragment plasmids were constructed. (G) Extracts of HEK293T cells transfected with functional truncations of His-USP7 plasmids (208-1102aa, 1-801aa, 208-801aa, 1-560aa, 208-560aa) or Flag-ER $\beta$  plasmids were immuno precipitated with anti-His magnetic beads.

Then, we generated several functional truncations of ER $\beta$  protein (1-248aa, 248-530aa, 1-149aa, 1-214aa, 149-530aa, 214-530aa, 149-248aa and 149-214aa) and USP7 protein (208-1102aa, 1-801aa, 208-801aa, 1-560aa, 208-560aa), respectively (Fig. 5F and S3C). Our data showed that the C-D (149-248aa) regions constituted an ER $\beta$  domain that interacts with USP7 (Fig. 5E). Next, we identified the USP7 domain that interacts with ER $\beta$  and found that ER $\beta$  interacts with the MATH (1-208aa) and UBL (801-1102aa) domains of USP7 (Fig. 5G). Altogether, the results of these assays strongly support the notion that the MATH (1-208aa) and UBL (801-1102aa) domains of USP7 directly interact with the C-D (149-248aa) domains of ER $\beta$ .

### **3.6. USP7-promoted ER $\beta$ stabilization is potentiated by ROS-induced stimulation**

Given that the deubiquitinase USP7 functions solely by deubiquitinating substrates [37], USP7 mediation of ER $\beta$  stability via the ubiquitin–proteasome (UPS) pathway is a reasonable explanation. As shown in Fig. 6A, we found that USP7 reduced the number of polyubiquitinated chains on ER $\beta$ . Consistently, USP7 overexpression extended the half-life of the ER $\beta$  protein (Fig. 6B and C). In addition, the expression of ER $\beta$  protein was upregulated after USP7 overexpression, but its mRNA level was unchanged in HCC827 and H1975 cells (Figs. S6A–C). In contrast, USP7-mediated ER $\beta$  deubiquitylation was reversed after treating with USP7 inhibitors P5091. (Fig. 6D). In addition, proteasome inhibitor



(caption on next page)

**Fig. 6.** USP7-promoted ER $\beta$  stabilization is potentiated by ROS-induced stimulation. (A) HEK293T cells were transfected with indicated plasmids for 72 h and treated with MG132 (20  $\mu$ M) for another 8 h. Cellular extracts were immunoprecipitated with anti-Flag magnetic beads. (B) HCC827 and H1975 cells transfected with vector or His-USP7 plasmids. The cells were treated with cycloheximide (CHX) and collected at the indicated time points for use in Western blot. (C) At each time point, the intensity of ER $\beta$  was normalized to the intensity of GAPDH (the loading control) first and then to the value at the 0-min time point. (D) HEK293T cells were transfected with plasmids and treated with or without P5091 (10  $\mu$ M) for 72 h and MG132 (20  $\mu$ M) for another 8 h. Cellular extracts were immunoprecipitated with anti-Flag magnetic beads. (E) HCC827OR and H1975OR cells were treated with or without P5091 (10  $\mu$ M) for 72 h and MG132 (20  $\mu$ M) for another 8 h. The expression of the indicated proteins was measured by Western blot. (F) HEK293T cells were transfected with indicated plasmids (His-USP7, Flag-ER $\beta$ , HA-UB WT, HA-UB K48R, or HA-UB K63R) for 72 h and treated with MG132 (20  $\mu$ M) for another 8 h. Cellular extracts were immunoprecipitated with anti-Flag magnetic beads and ubiquitination assay was used to detect the ubiquitination level of Flag-ER $\beta$ . (G) HEK293T cells were transfected with indicated plasmids (Flag-ER $\beta$ , HA-UB WT, His-USP7 full-length, His-USP7 206-1102aa, or His-USP7 1-560aa) for 72 h and treated with MG132 (20  $\mu$ M) for another 8 h. Cellular extracts were immunoprecipitated with anti-Flag magnetic beads and ubiquitination assay was used to detect the ubiquitination level of Flag-ER $\beta$ . (H) HEK293T cells were transfected with indicated plasmids (Flag-ER $\beta$ , HA-UB WT, His-USP7 WT, or His-USP7 C223S) for 72 h and treated with MG132 (20  $\mu$ M) for another 8 h. Cellular extracts were immunoprecipitated with anti-Flag magnetic beads and ubiquitination assay was used to detect the ubiquitination level of Flag-ER $\beta$ . (I) NSCLC cells were transfected with plasmids and treated with or without H<sub>2</sub>O<sub>2</sub> (200  $\mu$ M) for 120 min. Cellular extracts were immunoprecipitated with anti-Flag magnetic beads. (J) HCC827 cells were transfected with siRNAs (siControl, siUSP7) for 72 h and treated with or without H<sub>2</sub>O<sub>2</sub> (200  $\mu$ M) for another 120 min. The expression of the indicated proteins was measured by Western blotting. (K) HCC827 cells were treated with or without P5091 (10  $\mu$ M) for 72 h and H<sub>2</sub>O<sub>2</sub> (200  $\mu$ M) for another 120 min. The expression of the indicated proteins was measured by Western blotting. (L) Extracts of NSCLC cells treated with or without H<sub>2</sub>O<sub>2</sub> (200  $\mu$ M) for 120 min were immunoprecipitated with IgG and USP7 antibodies. Error bars represent the mean ( $n = 3$ )  $\pm$  S.D. ns p > 0.05, \*p < 0.05, \*\*p < 0.01, and \*\*\*p < 0.001.

MG132 reversed the inhibitory effect of P5091 on ER $\beta$  protein level, suggesting that USP7 upregulates ER $\beta$  protein via suppressing proteasomal degradation (Fig. 6E). Recent study revealed that K48- and K63-polyubiquitin were the two best characterized ubiquitin linkages cleaved by USP7 [41,42]. In our study, we replaced K48 or K63 lysine residue with an arginine residue and revealed that K48-linked ubiquitinated ER $\beta$  was the major form of ubiquitination inhibited by USP7 action (Fig. 6F). Interestingly, USP7 mutants lacking the UBL (560-1102aa) domain removed ubiquitin from ER $\beta$  but mutants lacking the MATH (1-208aa) domain could not remove ubiquitin (Fig. 6G). In addition, we found that USP7-WT but not the catalytically inactive mutant USP7-C223S reduced the number of polyubiquitin chains on ER $\beta$ , implying that the enzymatic activity of USP7 was required for ER $\beta$  stabilization (Fig. 6H).

To determine the role of ROS in USP7-promoted ER $\beta$  stabilization, we first performed co-IP assays and found that H<sub>2</sub>O<sub>2</sub> largely attenuated ER $\beta$  ubiquitination (Fig. 6I). In addition, a significant increase in endogenous ER $\beta$  protein level, an extended protein half-life and unaffected mRNA abundance confirmed this result (Figs. S6D–G). Notably, we found that H<sub>2</sub>O<sub>2</sub>-induced ER $\beta$  upregulation was abrogated after USP7 knockdown (Fig. 6J and S6H). P5091 treatment also showed similar effects (Fig. 6K and S6I). Furthermore, H<sub>2</sub>O<sub>2</sub> markedly enhanced the interaction of USP7 with ER $\beta$  (Fig. 6L). These results indicate that the physical interaction and functional connection between ER $\beta$  and USP7 are strengthened by ROS.

### 3.7. USP7 silencing induces ROS accumulation and overcomes osimertinib resistance by destabilizing ER $\beta$

We have shown that ER $\beta$  functions in ROS accumulation and osimertinib resistance in NSCLC cells and therefore explored whether USP7 is involved in mitigating ROS accumulation and promoting osimertinib resistance by stabilizing ER $\beta$ . We knocked down USP7 with siRNA in HCC827OR and H1975OR cells and found that USP7 knockdown resulted in a decrease in ER $\beta$  protein (Fig. 7A and S7A). DCFH-DA and JC-1 assays showed that osimertinib-induced ROS levels and loss of  $\Delta\Psi_m$  were also significantly increased following USP7 knockdown (Fig. 7B, C and S7B, C). Cell apoptosis in osimertinib-treated HCC827OR and H1975OR cells was induced following USP7 knockdown (Fig. 7D and S7D). In addition, CCK8 assays exhibited that USP7 knockdown in HCC827OR and H1975OR cells decreased the IC<sub>50</sub> for osimertinib (Fig. 7E and S7E). Then, we reintroduced ER $\beta$  protein in USP7-silenced cells (Fig. 7A and S7A). Notably, the elevation in ROS levels and loss of  $\Delta\Psi_m$  through USP7 knockdown was partially rescued by ER $\beta$  re-introduction (Fig. 7B, C and S7B, C). Meanwhile, restoring ER $\beta$  expression in USP7-silenced cells partially reversed the cell apoptosis rate and osimertinib sensitivity (Fig. 7D, E and S7D, E). Overall, these results

suggested that genetic inhibition of USP7 promoted ROS accumulation and overcame osimertinib resistance by destabilizing ER $\beta$  in NSCLC.

## 4. Discussion

Osimertinib has been clinically effective for controlling advanced NSCLC with EGFR mutations [43]. Unfortunately, acquired resistance curtails its efficacy. In our study, we found that promoting ROS accumulation is a potential strategy to overcome osimertinib resistance in NSCLC. More importantly, we provided strong evidence supporting a novel role for ER $\beta$  in mitigating ROS accumulation and promoting osimertinib resistance through the suppression of PRDX3 SUMOylation in NSCLC. Furthermore, we identified USP7 as a novel binding partner that deubiquitinates and stabilizes ER $\beta$ . In addition, we found that depletion of ER $\beta$  induced ROS accumulation and overcame osimertinib resistance both in vitro and in vivo. Therefore, targeting ER $\beta$  may be a novel strategy to overcome osimertinib resistance in NSCLC.

Based on an increasing body of evidence, ROS is considered an important participant of drug resistance in cancer cells [44]. However, work still needed to identify key molecules that regulated ROS level, as these molecules may serve as therapeutic targets to overcome osimertinib resistance. In this study, we revealed that ER $\beta$  is a novel regulator that specifically controls ROS accumulation, which overcomes osimertinib resistance in NSCLC. However, the upstream regulatory mechanisms of ER $\beta$  expression remain unclear. Here, for the first time, we identified USP7 as a novel upstream modulator that deubiquitinates the ER $\beta$  protein and thus maintains its stability at the posttranslational level. In addition, our results identified the MATH and UBL domains of USP7 and the C-D regions of ER $\beta$  as critical for the interaction of these two proteins. In this study, we also revealed that USP7 preferentially cleaved the K48-polyubiquitin chain on the ER $\beta$  protein and subsequently prevented ER $\beta$  proteasomal degradation. Moreover, USP7 was shown to be involved in mediating ROS accumulation and promoting osimertinib resistance in an ER $\beta$ -dependent manner in NSCLC. In aggregate, our results suggest that USP7 is a novel bona fide deubiquitinase of the ER $\beta$  protein that increases its stability and that ER $\beta$  is an oncogene that facilitates osimertinib resistance in NSCLC.

The molecular mechanisms underlying the role played by ER $\beta$  in osimertinib resistance remains unclear in NSCLC. In this study, we found that ER $\beta$  physically and specifically interacts with PRDX3 in mitochondria. Interestingly, we also uncovered that ROS stimulated ER $\beta$  translocation to mitochondria. Moreover, the interaction of ER $\beta$  and PRDX3 in mitochondria was enhanced by ROS. As one of the PRDX isoforms, PRDX3 is exclusively localized to mitochondria, where it is abundant [45]. More importantly, PRDX3 protects cells from ROS accumulation by eliminating approximately 90 % of cellular H<sub>2</sub>O<sub>2</sub> [46]. In our study, our results indicated that ER $\beta$  promoted osimertinib

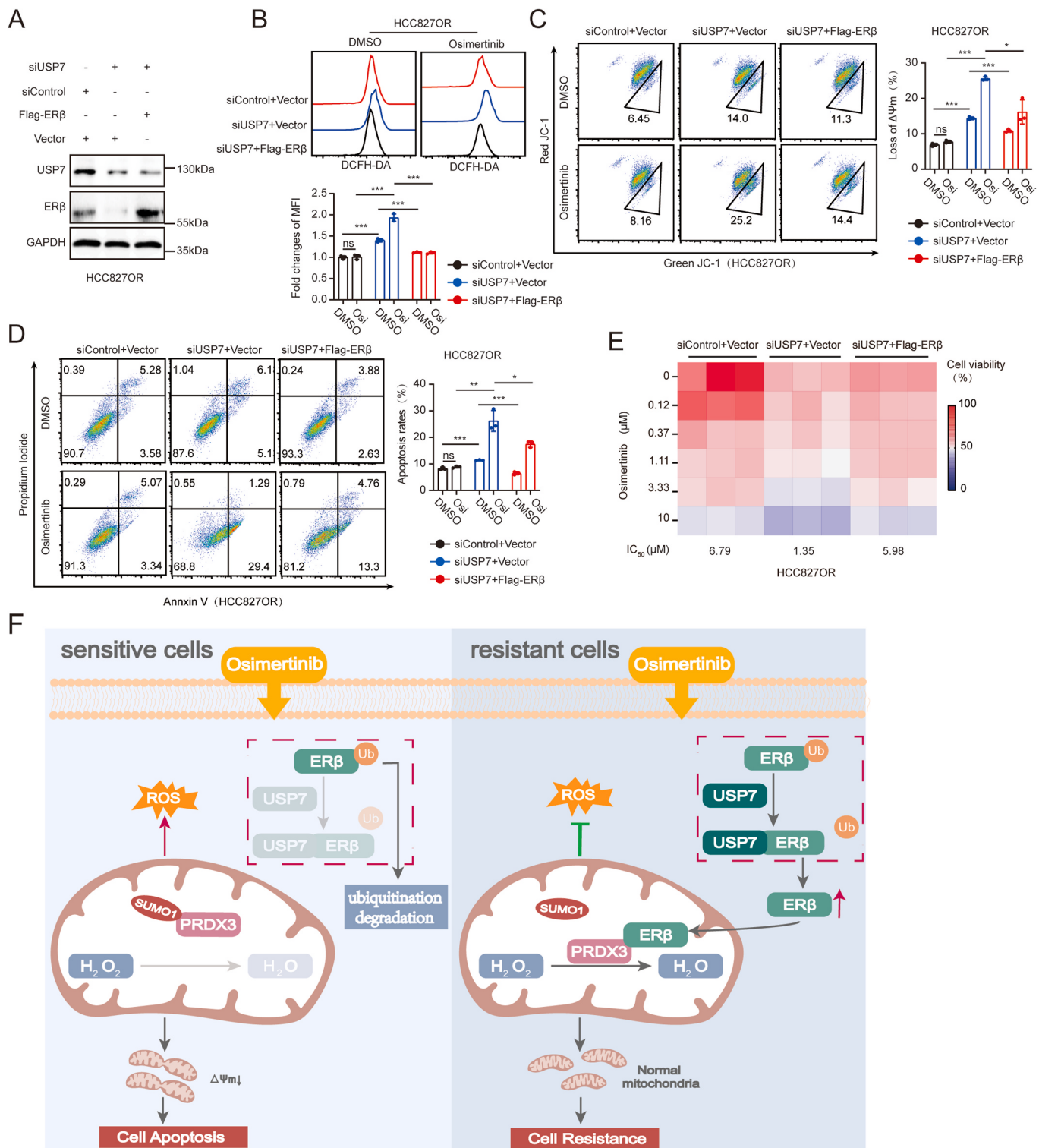


**Fig. 7.** USP7 silencing induces ROS accumulation and overcomes osimertinib resistance by destabilizing ER $\beta$  in NSCLC. (A) HCC827OR were transfected with indicated siRNAs (siControl, siUSP7) or plasmids (vector, Flag-ER $\beta$ ) for 72 h. The expression of the indicated proteins was measured via Western blot. (B-D) HCC827OR cells were transfected with indicated siRNAs (siControl, siUSP7) or plasmids (vector, Flag-ER $\beta$ ) for 72 h and treated with DMSO or osimertinib (1  $\mu$ M) for another 48 h. Then, these cells were collected for DCFH-DA (B), JC-1 (C), and Annexin-V/PI (D) flow cytometry assays. (E) HCC827OR cells were transfected with indicated siRNAs (siControl, siUSP7) or plasmids (vector, Flag-ER $\beta$ ) for 72 h and treated with a serial dose of osimertinib. Then, these cells were collected for CCK-8 assay and subjected to measure the IC<sub>50</sub> values of osimertinib. (F) Schematic representation showing USP7-mediated ER $\beta$  stabilization in suppressed PRDX3 SUMOylation to mitigate ROS accumulation and promote osimertinib resistance in NSCLC. Error bars represent the mean ( $n = 3$ )  $\pm$  S.D. ns p > 0.05, \*p < 0.05, \*\*p < 0.01, and \*\*\*p < 0.001.

resistance through its interaction with PRDX3 in NSCLC.

As a key PTM, SUMOylation is a critical event in the dynamic regulation of drug resistance [17]. In our study, we are the first to reveal that PRDX3 was modified via SUMOylation in a UBC9-dependent manner. Moreover, the SUMOylation inhibitor 2-D08 weakened the ability of osimertinib to elevate ROS levels and kill NSCLC cells, indicating that SUMOylation inhibit the ROS clearance capability of PRDX3. We also showed that ER $\beta$  played an essential role in suppressing PRDX3 SUMOylation by competing with UBC9 for binding to PRDX3. In addition, PRDX3 silencing increased the promotional effect of osimertinib on ROS accumulation in ER $\beta$ -overexpressed NSCLC cells. Together, our results suggest that ER $\beta$  mitigates ROS accumulation and promotes osimertinib resistance by suppressing PRDX3 SUMOylation.

In conclusion, USP7-mediated ER $\beta$  stabilization mitigates ROS accumulation and promotes osimertinib resistance by suppressing PRDX3 SUMOylation in non-small cell lung carcinoma (Fig. 7F), not only shedding light on the molecular regulatory mechanism underlying ER $\beta$  cause of osimertinib resistance but also implying that ER $\beta$  is a promising target for combination therapies to overcome osimertinib resistance in patients with NSCLC.

## Funding statement

This work was supported by grants from National Natural Science Foundation of China (81572277, 82072593, 82303353).

## Availability of data and materials

All the relevant data supporting the findings of this study are available within the article and its supplementary information files or from the corresponding author upon reasonable request.

## CRediT authorship contribution statement

**Yunchong Meng:** Writing – review & editing, Writing – original draft, Formal analysis, Data curation. **Wei Lin:** Writing – review & editing, Visualization, Validation, Formal analysis, Data curation. **Na Wang:** Resources, Methodology, Investigation, Conceptualization. **Xiao Wei:** Visualization, Methodology. **Peiyuan Mei:** Visualization, Supervision, Software, Conceptualization. **Xiaojun Wang:** Writing – review & editing, Conceptualization. **Chi Zhang:** Formal analysis, Conceptualization. **Quanfu Huang:** Writing – review & editing, Visualization, Investigation, Conceptualization. **Yongde Liao:** Writing – review & editing, Writing – original draft, Project administration, Funding acquisition, Conceptualization.

## Declaration of competing interest

I confirm that the contents of this manuscript have not been copyrighted or published previously, and that the manuscript is not under consideration for publication elsewhere. The authors declare no competing interests. All authors participated in the management of the patient described in the report. In addition, all participated in the writing and/or critical review of the manuscript, and all have read and approved the final version submitted.

## Acknowledgments

None.

## Appendix A. Supplementary data

Supplementary data to this article can be found online at <https://doi.org/10.1016/j.canlet.2023.216587>.

## References

- [1] F. Bray, J. Ferlay, I. Soerjomataram, R.L. Siegel, L.A. Torre, A. Jemal, Global cancer statistics 2018: GLOBOCAN estimates of incidence and mortality worldwide for 36 cancers in 185 countries, CA A Cancer J. Clin. 68 (2018) 394–424.
- [2] R.L. Siegel, K.D. Miller, A. Jemal, Cancer statistics, 2020, CA A Cancer J. Clin. 70 (2020) 7–30.
- [3] D.S. Ettinger, D.E. Wood, D.L. Aisner, W. Akerley, J.R. Bauman, A. Bharat, D. S. Bruno, et al., NCCN Guidelines® insights: non-small cell lung cancer, version 2.2023, J. Natl. Compr. Cancer Netw. 21 (2023) 340–350.
- [4] R. Rosell, T. Moran, C. Queralt, R. Porta, F. Cardenal, C. Camps, M. Majem, et al., Screening for epidermal growth factor receptor mutations in lung cancer, N. Engl. J. Med. 361 (2009) 958–967.
- [5] J.C. Soria, Y. Ohe, J. Vansteenkiste, T. Reungwetwattana, B. Chewaskulyong, K. H. Lee, A. Dechaphunkul, et al., Osimertinib in untreated EGFR-mutated advanced non-small-cell lung cancer, N. Engl. J. Med. 378 (2018) 113–125.
- [6] B. D'Autréaux, M.B. Toledo, ROS as signalling molecules: mechanisms that generate specificity in ROS homeostasis, Nat. Rev. Mol. Cell Biol. 8 (2007) 813–824.
- [7] E.C. Cheung, K.H. Vousden, The role of ROS in tumour development and progression, Nat. Rev. Cancer 22 (2022) 280–297.
- [8] J.D. Hayes, A.T. Dinkova-Kostova, K.D. Tew, Oxidative stress in cancer, Cancer Cell 38 (2020) 167–197.
- [9] Y. Hao, T.F. Langford, S.J. Moon, K.A. Eller, H.D. Sikes, Screening compound libraries for H<sub>2</sub>O<sub>2</sub>-mediated cancer therapeutics using a peroxiredoxin-based sensor, Cell Chem. Biol. 29 (2022) 625–635.
- [10] Q. Cui, J.Q. Wang, Y.G. Assaraf, L. Ren, P. Gupta, L. Wei, et al., Modulating ROS to overcome multidrug resistance in cancer, Drug Resist. Updates 41 (2018) 1–25.
- [11] J. Bolduc, K. Koruza, T. Luo, J. Malo Pueyo, T.N. Vo, D. Ezerina, et al., Peroxiredoxins wear many hats: factors that fashion their peroxide sensing personalities, Redox Biol. 42 (2021), 101959.
- [12] H. Huang, S. Zhang, Y. Li, Z. Liu, L. Mi, Y. Cai, et al., Suppression of mitochondrial ROS by prohibitin drives glioblastoma progression and therapeutic resistance, Nat. Commun. 12 (2021) 3720.
- [13] Z. Wang, R. Sun, G. Wang, Z. Chen, Y. Li, Y. Zhao, et al., SIRT3-mediated deacetylation of PRDX3 alleviates mitochondrial oxidative damage and apoptosis induced by intestinal ischemia/reperfusion injury, Redox Biol. 28 (2020), 101343.
- [14] S. Elumalai, U. Karunakaran, J.S. Moon, K.C. Won, High glucose-induced PRDX3 acetylation contributes to glucotoxicity in pancreatic  $\beta$ -cells: prevention by Teneliglitin, Free Radic. Biol. Med. 160 (2020) 618–629.
- [15] A.C.O. Vertegaal, Signalling mechanisms and cellular functions of SUMO, Nat. Rev. Mol. Cell Biol. 23 (2022) 715–731.
- [16] M. Basu-Shrivastava, B. Mojsa, S. Mora, I. Robbins, G. Bossis, I. Lassot, et al., Trim39 regulates neuronal apoptosis by acting as a SUMO-targeted E3 ubiquitin-ligase for the transcription factor NFATc3, Cell Death Differ. 29 (2022) 2107–2122.
- [17] X. Shangguan, J. He, Z. Ma, W. Zhang, Y. Ji, K. Shen, et al., SUMOylation controls the binding of hexokinase 2 to mitochondria and protects against prostate cancer tumorigenesis, Nat. Commun. 12 (2021) 1812.
- [18] S. Liu, C. Hu, M. Li, J. An, W. Zhou, J. Guo, et al., Estrogen receptor beta promotes lung cancer invasion via increasing CXCR4 expression, Cell Death Dis. 13 (2022) 70.
- [19] W. Yu, J. Ding, M. He, Y. Chen, R. Wang, Z. Han, et al., Estrogen receptor  $\beta$  promotes the vasculogenic mimicry (VM) and cell invasion via altering the lncRNA-MALAT1/miR-145-5p/NEDD9 signals in lung cancer, Oncogene 38 (2019) 1225–1238.
- [20] M. He, H. Yang, H. Shi, Y. Hu, C. Chang, S. Liu, et al., Sunitinib increases the cancer stem cells and vasculogenic mimicry formation via modulating the lncRNA-ECVSR/ER $\beta$ /Hif2- $\alpha$  signaling, Cancer Lett. 524 (2022) 15–28.
- [21] B. Xie, Q. Meng, H. Yu, K. Shen, Y. Cheng, C. Dong, et al., Estrogen receptor  $\beta$ -targeted hypoxia-responsive near-infrared fluorescence probes for prostate cancer study, Eur. J. Med. Chem. 238 (2022), 114506.
- [22] Q. Meng, B. Xie, H. Yu, K. Shen, X. Deng, H.B. Zhou, et al., Estrogen receptor  $\beta$ -targeted near-infrared inherently fluorescent probe: a potent tool for estrogen receptor  $\beta$  research, ACS Sens. 7 (2022) 109–115.
- [23] L.P. Stabile, S. Dacic, S.R. Land, D.E. Lenzner, R. Dhir, M. Acquafonda, et al., Combined analysis of estrogen receptor beta-1 and progesterone receptor expression identifies lung cancer patients with poor outcome, Clin. Cancer Res. 17 (2011) 154–164.
- [24] B. Xie, Q. Meng, H. Yu, K. Shen, Y. Cheng, C. Dong, et al., Estrogen receptor  $\beta$ -targeted hypoxia-responsive near-infrared fluorescence probes for prostate cancer study, Eur. J. Med. Chem. 238 (2022), 114506.
- [25] H. Jiang, X.W. Zhang, Q.L. Liao, W.T. Wu, Y.L. Liu, W.H. Huang, Electrochemical monitoring of paclitaxel-induced ROS release from mitochondria inside single cells, Small 15 (2019), e1901787.
- [26] Y. Meng, W. Lin, N. Wang, X. Wei, Q. Huang, Y. Liao, Bazedoxifene-induced ROS promote mitochondrial dysfunction and enhance osimertinib sensitivity by inhibiting the p-STAT3/SOCS3 and KEAP1/NRF2 pathways in non-small cell lung cancer, Free Radic. Biol. Med. 196 (2023) 65–80.
- [27] Q. Huang, Q. Wang, D. Li, X. Wei, Y. Jia, Z. Zhang, et al., Co-administration of 20 (S)-protopanaxatriol (g-PPT) and EGFR-TKI overcomes EGFR-TKI resistance by decreasing SCDF1 induced lipid accumulation in non-small cell lung cancer, J. Exp. Clin. Cancer Res. 38 (2019) 129.
- [28] D. Bazopoulou, D. Knoefler, Y. Zheng, K. Ulrich, B.J. Oleson, L. Xie, et al., Developmental ROS individualizes organismal stress resistance and lifespan, Nature 576 (2019) 301–305.

- [29] H. Sies, D.P. Jones, Reactive oxygen species (ROS) as pleiotropic physiological signalling agents, *Nat. Rev. Mol. Cell Biol.* 21 (2020) 363–383.
- [30] S. Gandhi, A. Wood-Kaczmar, Z. Yao, H. Plun-Favreau, E. Deas, K. Klupsch, et al., PINK1-associated Parkinson's disease is caused by neuronal vulnerability to calcium-induced cell death, *Mol. Cell* 33 (2009) 627–638.
- [31] A. Chandrasekharan, S.N. Varadarajan, A. Lekshmi, S.S. Lupitha, P. Darvin, L. Chandrasekhar, et al., A high-throughput real-time in vitro assay using mitochondrial targeted roGFP for screening of drugs targeting mitochondria, *Redox Biol.* 20 (2019) 379–389.
- [32] Y. Liu, W. She, Y. Li, M. Wang, Y. Liu, B. Ning, T. Xu, et al., Aa-Z2 triggers ROS-induced apoptosis of osteosarcoma by targeting PDK-1, *J. Transl. Med.* 21 (2023) 7.
- [33] Q. Huang, Z. Zhang, Y. Liao, C. Liu, S. Fan, X. Wei, et al., 17 $\beta$ -estradiol upregulates IL6 expression through the ER $\beta$  pathway to promote lung adenocarcinoma progression, *J. Exp. Clin. Cancer Res.* 37 (2018) 133.
- [34] A.T. Dharmaraja, Role of reactive oxygen species (ROS) in therapeutics and drug resistance in cancer and bacteria, *J. Med. Chem.* 60 (2017) 3221–3240.
- [35] D.R. Wonsey, K.I. Zeller, C.V. Dang, The c-Myc target gene PRDX3 is required for mitochondrial homeostasis and neoplastic transformation, *Proc. Natl. Acad. Sci. U. S. A.* 99 (2002) 6649–6654.
- [36] S.K. Sonn, E.J. Song, S. Seo, Y.Y. Kim, J.H. Um, F.J. Yeo, et al., Peroxiredoxin 3 deficiency induces cardiac hypertrophy and dysfunction by impaired mitochondrial quality control, *Redox Biol.* 51 (2022), 102275.
- [37] H. Yamamoto-Imoto, S. Minami, T. Shioda, Y. Yamashita, S. Sakai, S. Maeda, et al., Age-associated decline of MondoA drives cellular senescence through impaired autophagy and mitochondrial homeostasis, *Cell Rep.* 38 (2022), 110444.
- [38] Z. Hu, X.L. Teng, T. Zhang, X. Yu, R. Ding, J. Yi, et al., SENP3 senses oxidative stress to facilitate STING-dependent dendritic cell antitumor function, *Mol. Cell* 81 (2021) 940–952.
- [39] J.S. Seeler, A. Dejean, SUMO and the robustness of cancer, *Nat. Rev. Cancer* 17 (2017) 184–197.
- [40] A.R. Cox, N. Chernis, K.H. Kim, P.M. Masschelin, P.K. Saha, S.M. Briley, et al., Ube2i deletion in adipocytes causes lipodystrophy in mice, *Mol. Metabol.* 48 (2021), 101221.
- [41] L. Ji, B. Lu, R. Zamponi, O. Charlat, R. Aversa, Z. Yang, et al., USP7 inhibits Wnt/ $\beta$ -catenin signaling through promoting stabilization of Axin, *Nat. Commun.* 10 (2019) 4184.
- [42] L. Liang, Y. Peng, J. Zhang, Y. Zhang, M. Roy, X. Han, et al., Deubiquitylase USP7 regulates human terminal erythroid differentiation by stabilizing GATA1, *Haematologica* 104 (2019) 2178–2187.
- [43] J. Remon, C.E. Steuer, S.S. Ramalingam, E. Felip, Osimertinib and other third-generation EGFR TKI in EGFR-mutant NSCLC patients, *Ann. Oncol.* 29 (2018) i20–i27.
- [44] J. Xu, L. Ji, Y. Ruan, Z. Wan, Z. Lin, S. Xia, et al., UBQLN1 mediates sorafenib resistance through regulating mitochondrial biogenesis and ROS homeostasis by targeting PGC1 $\beta$  in hepatocellular carcinoma, *Signal Transduct. Targeted Ther.* 6 (2021) 190.
- [45] Z. Liu, Y. Hu, Y. Gong, W. Zhang, C. Liu, Q. Wang, et al., Hydrogen peroxide mediated mitochondrial UNG1-PRDX3 interaction and UNG1 degradation, *Free Radic. Biol. Med.* 99 (2016) 54–62.
- [46] T. Ismail, Y. Kim, H. Lee, D.S. Lee, H.S. Lee, Interplay between mitochondrial peroxiredoxins and ROS in cancer development and progression, *Int. J. Mol. Sci.* 20 (2019) 4407.